Dilepton production from chirally asymmetric matter

Nilanjan Chaudhuri,[1,2,*] Snigdha Ghosh,[3,†] Sourav Sarkar,[1,2,‡] and Pradip Roy[4,2,§]

[1]*Variable Energy Cyclotron Centre, 1/AF Bidhannagar, Kolkata 700064, India*
[2]*Homi Bhabha National Institute, Training School Complex, Anushaktinagar, Mumbai 400094, India*
[3]*Government General Degree College Kharagpur-II, Paschim Medinipur, West Bengal 721149, India*
[4]*Saha Institute of Nuclear Physics, 1/AF Bidhannagar, Kolkata 700064, India*

(Received 19 January 2022; accepted 2 April 2022; published 2 May 2022)

We evaluate the dilepton production rate (DPR) from hot and dense chirally asymmetric quark matter. The presence of a finite chiral chemical potential (CCP) in the electromagnetic spectral function results in the appearance of new cut structures signifying additional scattering processes in the medium which leads to a significant enhancement in the DPR at lower values of invariant mass. The constituent quark mass evaluated using a three-flavor Nambu–Jona-Lasinio model is also nontrivially affected by the CCP. These are found to result in a continuous dilepton production rate as a function of the invariant mass for higher values of temperature and baryonic chemical potential.

DOI: 10.1103/PhysRevD.105.096001

I. INTRODUCTION

The study of QCD vacuum structure under extreme conditions of temperature and/or baryon density is one of the main objectives of relativistic heavy ion collision (HIC) experiments at the RHIC and LHC. It is well established that the infinite number of energy-degenerate different vacuum configurations of QCD at zero and low temperatures can be characterized by topologically nontrivial gauge configurations with a nonzero winding number [1]. These gluon configurations are called instantons which can invoke transition between two different vacua by means of crossing a potential barrier with a height of the order of the QCD scale Λ_{QCD}. This mechanism is known as instanton tunnelling [2–4]. However, at high temperatures, for example, in the quark gluon plasma (QGP) phase of HICs, a copious production of another kind of gluon configuration, called sphalerons, is expected [5,6]. It is conjectured that the abundance of sphalerons can enhance the transition rate by crossing the barriers between different energy-degenerate vacua [7–10]. The topologically nontrivial gauge field configurations can switch the helicities of quarks while interacting with them. This in turn leads to the breaking of parity (P) and charge-parity (CP) symmetries by creating an asymmetry between left- and right-handed quarks via the axial anomaly of QCD [11,12]. Chirality imbalance can be produced locally as there is no direct observation of the violation of P and CP in QCD globally [11–14]. This locally induced chirality imbalance is characterized by means of a chiral chemical potential (CCP) which basically represents the difference between the number of right- and left-handed quarks.

HICs with a nonzero impact parameter can give rise to very high magnetic fields of the order of few m_π^2 [15,16]. Such high magnetic fields in the presence of chirality imbalance can lead to a separation of positive and negative charges with respect to the reaction plane and induce a current along the magnetic field dubbed as chiral magnetic effect (CME) [15,17–19]. Substantial efforts have been made to detect CME in HIC experiments at the RHIC at Brookhaven. Very recently, the STAR Collaboration has performed an extensive analysis which has provided no indication of CME in HICs [20]. As a consequence, new techniques for the experimental determination of CME have been proposed [21,22].

Since a local domain of chirality imbalance is expected to be produced in QGP, in addition to the CME there have been intense studies on the phase structure [23–25], microscopic transport phenomena [17,26–28], collective oscillations [29–31], fermion damping rate [32], and collisional energy loss of fermions [31], as well as properties of electromagnetic spectral function [33] in chirally imbalanced medium. Moreover, chirally asymmetric plasma is expected to be produced in the gap regions of the magnetospheres of pulsars and black holes [34] and other stellar astrophysical scenario [29,35–38].

*sovon.nilanjan@gmail.com; n.chaudhri@vecc.gov.in
†Corresponding author.
snigdha.physics@gmail.com
‡sourav@vecc.gov.in
§pradipk.roy@saha.ac.in

Furthermore, it is worthwhile to mention that a CME has indeed been observed in condensed matter systems, particularly in three-dimensional Dirac as well as Weyl semimetals [39–47]. Thus the study of the properties of chirally imbalanced matter continues to be a matter of major topical interest.

It is well known that the hot and dense matter produced in HICs cools via rapid expansion under its own pressure passing through different stages of evolution. However, the whole process is very transient (∼few fm/c), restricting the possibility of a direct observation. So to investigate microscopic as well as bulk properties of QGP one has to rely on indirect probes and observables [48]. Electromagnetic probes, photons, and dileptons have long been used as reliable probes of HICs. Because they participate only in electromagnetic interaction, their mean free paths are much larger than the typical size of the system. As a consequence, once produced they tend to leave the system without suffering further interactions, thus carrying unaltered information about the space-time region from where they are produced [49–59]. As the production rate of dileptons and photons is directly proportional to the electromagnetic spectral function, the study of its analytic properties is of central importance [48,53,59,60]. Such a study in chirally imbalanced hot and/or dense matter has recently been performed in [33], where a rich cut structure was revealed. The steplike structure of the spectral function observed in a certain invariant mass range were attributed to the thresholds of Unitary and Landau cuts indicating additional scattering processes in the medium. We expect that such structures will have nontrivial effects on the dilepton spectrum.

The imaginary part of the electromagnetic current correlator containing the modified quark propagators in the presence of a hot and dense medium is the most important component in the evaluation of the dilepton production rate (DPR), which determines the thresholds as well as the intensity of the emission of dileptons [52,53]. Thus, it has a crucial dependence in the value of quark mass. As the system cools, the quark condensate builds up due to the breaking of chiral symmetry which results in a large value of the quark mass (∼ few hundred MeV). The nonperturbative nature of QCD at low energies severely hinders the theoretical analysis of these phenomena using first principle calculations. As an alternative, we have used the Nambu–Jona-Lasinio (NJL) model [61,62] which is built by respecting the global symmetries of QCD, most importantly the chiral symmetry [63–65]. This model has been very useful in probing the vacuum structure of QCD at arbitrary values of temperature, baryon chemical potential (BCP), and CCP [66–72].

In this work, we shall evaluate the DPR from a (locally) chirally imbalanced quark matter expected to be produced in relativistic HIC experiments. We use the three-flavor NJL model to evaluate the constituent quark mass by solving the self-consistent gap equations. The quark mass for different flavors $M_f = M_f(T, \mu_B, \mu_5)$ will go as an input in the electromagnetic spectral function. We have made use of the analytic structure of the in-medium spectral function to obtain the thresholds of dilepton production due to various scattering processes involving quarks for both zero and nonzero values of μ_5.

The paper is organized as follows. In the next section we discuss the formulation of the dilepton production rate at zero and a finite value of the CCP. Next, we discuss in Sec. III the evaluation of the constituent quark mass from a three-flavor NJL model. Section IV deals with the numerical results followed by a summary and discussion in Sec. V.

II. DILEPTON PRODUCTION RATE

In QGP, a quark can interact with an antiquark to produce a virtual photon, which subsequently decays into a lepton l^+ and antilepton l^- pair (see Fig. 1). The DPR from a hot and dense medium is already calculated in Refs. [48,49,51,60,73,74]. But, for the sake of completeness, we will briefly demonstrate a few important steps. First, we consider an initial state $|\mathcal{I}\rangle = |I(p_I)\rangle$ of a quark/antiquark with momentum p_I moving towards a final state $|\mathcal{F}\rangle = |F(p_F), l^+(p_{l^+})l^-(p_{l^-})\rangle$, consisting of a quark/antiquark of momentum p_F plus a pair of leptons of momenta p_{l^+} and p_{l^-}, respectively. The probability amplitude for such a transition is $|\langle\mathcal{F}|\hat{\mathcal{S}}|\mathcal{I}\rangle|^2$, where $\hat{\mathcal{S}}$ is the scattering matrix expressed as

$$\hat{\mathcal{S}} = \mathcal{T}\left[\exp\left(i\int \mathcal{L}_{\rm int}(x)d^4x\right)\right], \tag{1}$$

in which $\mathcal{T}$ is the time-ordering operator and

$$\mathcal{L}_{\rm int}(x) = j^\mu(x)A_\mu(x) + J^\mu(x)A_\mu(x) \tag{2}$$

is the Lagrangian (density) for local interaction. Our choice of metric tensor is $g^{\mu\nu} = \mathrm{diag}(1,-1,-1,-1)$. In the above

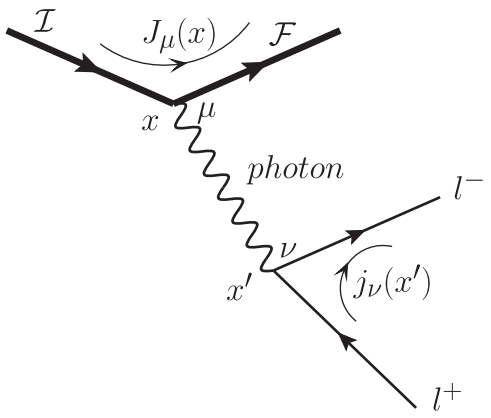

FIG. 1. Diagrammatic representation of the dilepton production amplitude.

equation, the conserved vector currents corresponding to the leptons and quarks denoted by $j^\mu(x)$ and $J^\mu(x)$, respectively, are coupled to the photon field represented by $A^\mu(x)$. It can be shown that the first nontrivial contribution to the above mentioned process comes from the second-order term in the $\hat{S}$ matrix expansion and the expression of the squared amplitude $|\langle\mathcal{F}|\hat{S}|\mathcal{I}\rangle|^2$ is given by

$$\begin{aligned}|\langle\mathcal{F}|\hat{S}|\mathcal{I}\rangle|^2 = \int\int d^4x' d^4x e^{i(p_{l^+}+p_{l^-})\cdot x'} \frac{1}{(p_{l^+}+p_{l^-})^4} \\ \times \langle l^+(p_{l^+}) l^-(p_{l^-})|j^\mu(0)|0\rangle \\ \times \langle 0|j^{\nu\dagger}(0)|l^+(p_{l^+}) l^-(p_{l^-})\rangle \\ \times \langle F(p_F)|J_\mu(x')|I(p_I)\rangle\langle I(p_I)|J^\dagger_\nu(0)|F(p_F)\rangle.\end{aligned} \tag{3}$$

Now the dilepton multiplicity from the thermal QGP medium is expressed as [60]

$$\begin{aligned}N = \frac{1}{\mathcal{Z}}\sum_{\text{spins}}\int\frac{d^3p_{l^+}}{(2\pi)^3 2p^0_{l^+}}\int\frac{d^3p_{l^-}}{(2\pi)^3 2p^0_{l^-}} \\ \times \sum_{I,F}\exp(-\beta p^0_I)|\langle F|\hat{S}|I\rangle|^2,\end{aligned} \tag{4}$$

where $\mathcal{Z}$ is the partition function of the system and the summation signifies sum over all leptonic spin configurations. Using Eq. (3) in Eq. (4), and after some simplifications, we arrive at [74]

$$N = \int d^4x \int \frac{d^4q}{(2\pi)^4} e^{-\beta q^0}\frac{1}{q^4}\mathbb{W}_{+\mu\nu}(q)\mathbb{L}^{\mu\nu}_+(q), \tag{5}$$

where

$$\mathbb{W}^{\mu\nu}_+(q) = \int d^4x e^{iq\cdot x}\langle J^\mu(x)J^{\nu\dagger}(0)\rangle, \tag{6}$$

$$\mathbb{L}^{\mu\nu}_+(q) = \int d^4x e^{iq\cdot x}\langle 0|j^{\nu\dagger}(x)j^\mu(0)|0\rangle. \tag{7}$$

Here $\langle\ldots\rangle$ represents the ensemble average and $q = (p_{l^+} + p_{l^-})$ is the total momentum of the lepton pair. So, the DPR becomes

$$\text{DPR} = \frac{dN}{d^4x d^4q} = \frac{1}{(2\pi)^4}\frac{e^{-\beta q^0}}{q^4}\mathbb{W}_{+\mu\nu}(q)\mathbb{L}^{\mu\nu}_+(q). \tag{8}$$

Now to calculate the DPR in the presence of a medium it is useful to write both the $\mathbb{W}^{\mu\nu}_+(q)$ and $\mathbb{L}^{\mu\nu}_+(q)$ in terms of time-ordered correlation functions so that one can apply the real-time formulation of the finite temperature field theory [60,74–76]. Thus, we get

$$\text{DPR} = \frac{dN}{d^4x d^4q} = \frac{1}{4\pi^4 q^4}\left(\frac{1}{e^{\beta q^0}+1}\right)\text{Im}\mathbb{W}^{\mu\nu}_{11}(q)\text{Im}\mathbb{L}_{\mu\nu}(q). \tag{9}$$

Until now we have not specified any explicit form of the currents $J^\mu(x)$ and $j^\mu(x)$, which are required to evaluate the quantities $\mathbb{W}^{\mu\nu}_{11}(q)$ and $\mathbb{L}^{\mu\nu}(q)$. In this work, we have considered

$$J^\mu(x) = e\bar{\mathrm{q}}(x)\hat{Q}\gamma^\mu \mathrm{q}(x), \tag{10}$$

$$j^\mu(x) = -e\bar{\psi}(x)\gamma^\mu\psi(x), \tag{11}$$

where $\mathrm{q} = (u\,d\,s)^T$ represents a three-flavor quark field multiplet with the corresponding charge matrix $\hat{Q} = \text{diag}(\frac{2}{3}, -\frac{1}{3}, -\frac{1}{3})$, ψ is the lepton field, and $e > 0$ is the absolute value of the electric charge of an electron. Using Eqs. (10) and (11) it can be shown that

$$\mathbb{W}^{\mu\nu}_{11}(q) = i\int\frac{d^4k}{(2\pi)^4}\text{Tr}_{\text{d,f,c}}[\gamma^\mu\hat{Q}S_{11}(p=q+k)\gamma^\nu\hat{Q}S_{11}(k)], \tag{12}$$

$$\mathbb{L}^{\mu\nu}(q) = ie^2\int\frac{d^4k}{(2\pi)^4}\text{Tr}_{\text{d}}[\gamma^\nu S(p=q+k)\gamma^\mu S(k)], \tag{13}$$

where the trace over Dirac, flavor, and color spaces are indicated by the subscript 'd', 'f', and 'c,' respectively, $S_{11}(p)$ is the 11-component of the real-time quark propagator, and $S(k)$ is the vacuum propagator for leptons with the Feynman boundary condition, which is expressed as

$$S(p) = \frac{-(\not{p}+m_L)}{p^2 - m_L^2 + i\varepsilon}, \tag{14}$$

with m_L being the mass of the lepton. It is to be noted that, in Eq. (12), the quark propagator $S_{11}(p)$ is diagonal in both the flavor and color space, i.e.,

$$S_{11}(p) = \text{diag}(S^u_{11}(p), S^d_{11}(p), S^s_{11}(p)) \otimes 1_{\text{color}}. \tag{15}$$

Since both the currents $J^\mu(x)$ and $j^\mu(x)$ are conserved: $\partial_\mu J^\mu(x) = 0 = \partial_\mu j^\mu(x)$, consequently the matter tensor $\mathbb{W}^{\mu\nu}_{11}(q)$, as well as the leptonic tensor $\mathbb{L}^{\mu\nu}(q)$, are transverse to the momentum q^μ, i.e.,

$$q_\mu\mathbb{W}^{\mu\nu}_{11}(q) = 0 = q_\mu\mathbb{L}^{\mu\nu}(q). \tag{16}$$

These transversality conditions enforce the following Lorentz structure of $\mathbb{L}^{\mu\nu}(q)$:

$$\mathbb{L}^{\mu\nu}(q) = \left(g^{\mu\nu} - \frac{q^\mu q^\nu}{q^2}\right)\left(\frac{1}{3}g_{\rho\sigma}\mathbb{L}^{\rho\sigma}\right). \tag{17}$$

Putting this back in Eq. (9), and using the transversality condition for the matter tensor, we get the DPR as

$$\mathrm{DPR} = \left(\frac{dN}{d^4x d^4q}\right) = \frac{1}{12\pi^4 q^4}\left(\frac{1}{e^{q^0/T}+1}\right) g_{\mu\nu}\mathrm{Im}\mathbb{W}_{11}^{\mu\nu}(q) g_{\rho\sigma}\mathrm{Im}\mathbb{L}^{\rho\sigma}(q). \quad (18)$$

It is easy to check, by substituting Eq. (14) into Eq. (13), that

$$g_{\rho\sigma}\mathrm{Im}\mathbb{L}^{\rho\sigma}(q) = \frac{-e^2}{4\pi} q^2 \left(1+\frac{2m_L^2}{q^2}\right)\sqrt{1-\frac{4m_L^2}{q^2}}\Theta(q^2-4m_L^2). \quad (19)$$

The effects of finiteness of the CCP will be encoded in the matter tensor part of Eq. (18). Thus, we shall consider the following two cases.

A. DPR at $\mu_5 = 0$

To evaluate the matter part at finite temperature for vanishing values of CCP, one requires the 11-component of the real-time thermal quark propagator. In spectral representation, the later is given by [60]

$$S_{11}^f(p) = \int_{-\infty}^{\infty} \frac{dp_0'}{2\pi}\sigma'^f(p_0', \vec{p}) \times \left[\frac{1}{p_0' - p_0 - i\varepsilon} - 2\pi i \eta(p_0')\delta(p_0' - p_0)\right], \quad (20)$$

where $\sigma'^f(p_0, \vec{p}) = 2\pi \mathrm{sgn}(p_0)(\not{p} + M_f)\delta(p^2 - M_f^2)$ is the fermionic spectral function, with M_f being the constituent mass of a quark with flavor f, and $\eta(x)$ is the distribution-like function containing the true Fermi-Dirac thermal distributions $f^{\pm}(x)$ of the quarks given by

$$\eta(x) = \Theta(x) f^+(|x|) - \Theta(-x) f^-(|x|) + \Theta(-x) \quad \text{with} \quad f^{\pm}(x) = \left[\exp\left(\frac{x \mp \mu_B/3}{T}\right) + 1\right]^{-1}, \quad (21)$$

in which μ_B is the BCP. Now in the local rest frame of the medium, using Eqs. (20), (21), and (15) in Eq. (12) one gets, after some algebra,

$$\begin{aligned} g_{\mu\nu}\mathrm{Im}\mathbb{W}_{11}^{\mu\nu}(q) = N_c \sum_f e_f^2 \pi \int \frac{d^3k}{(2\pi)^3}\frac{1}{4\omega_k\omega_p} [&\{1 - f^-(\omega_k) - f^+(\omega_p) + 2f^-(\omega_k)f^+(\omega_p)\}\mathcal{N}(k^0 = -\omega_k)\delta(q^0 - \omega_k - \omega_p) \\ &+ \{1 - f^+(\omega_k) - f^-(\omega_p) + 2f^+(\omega_k)f^-(\omega_p)\}\mathcal{N}(k^0 = \omega_k)\delta(q^0 + \omega_k + \omega_p) \\ &+ \{-f^-(\omega_k) - f^-(\omega_p) + 2f^-(\omega_k)f^-(\omega_p)\}\mathcal{N}(k^0 = -\omega_k)\delta(q^0 - \omega_k + \omega_p) \\ &+ \{-f^+(\omega_k) - f^+(\omega_p) + 2f^+(\omega_k)f^+(\omega_p)\}\mathcal{N}(k^0 = \omega_k)\delta(q^0 + \omega_k - \omega_p)], \end{aligned} \quad (22)$$

where $e_f = q_f e$, $\omega_k = \sqrt{\vec{k}^2 + M_f^2}$, $\omega_p = \sqrt{\vec{p}^2 + M_f^2} = \sqrt{(\vec{q}+\vec{k})^2 + M_f^2}$, and $\mathcal{N}(q,k) = 8(k^2 + q\cdot k - 2M_f^2)$. Note that the first delta function appearing in Eq. (22), termed as the Unitary-I cut, represents the contribution from quark-antiquark annihilation to a positive-energy timelike virtual photon (and the corresponding time-reversed process where such a photon decays into a quark-antiquark pair). The delta function in the second term (the Unitary-II cut) corresponds to a similar process but the virtual photon is of negative energy. The last two delta functions, called the Landau cuts, which are purely medium-dependent contributions, stand for the scattering/emission processes such as absorption of a spacelike virtual photon by a quark/antiquark and the consequent time-reversed processes. It can be easily checked that the contributions from Unitary-I and Unitary-II cuts are nonzero in the kinematic regions $\sqrt{\vec{q}^2 + 4M_f^2} < q^0 < \infty$ and $-\infty < q^0 < -\sqrt{\vec{q}^2 + 4M_f^2}$, respectively. On the other hand, the kinematic domain for both the Landau cuts is in the spacelike region $|q^0| < |\vec{q}|$. This cut structure of $\mathrm{Im}\mathbb{W}_{11}^{\mu\nu}$ in the complex q^0-plane is depicted in Fig. 2. Since we are interested in the physical dileptons with positive energy and timelike four-momentum, i.e., $q^0 > 0$ and $q^2 > 0$, it follows that only the Unitary-I cut contributions are kinematically allowed. It should be noted that the kinematic domains are directly related to the constituent quark mass M_f and hence can be different for different flavors [74–76]. Now, with the physical restrictions previously mentioned, the $d^3k = |\vec{k}|^2 d|\vec{k}| d(\cos\theta) d\phi$ integral of Eq. (22) can be evaluated analytically [the $d(\cos\theta)$ integral has been performed using the Dirac delta functions present in the integrand and the $d\phi$ integral trivially gives a factor of 2π]. Using this result in Eq. (18), we finally arrive at the following analytical expression for the DPR at vanishing CCP [74,77]:

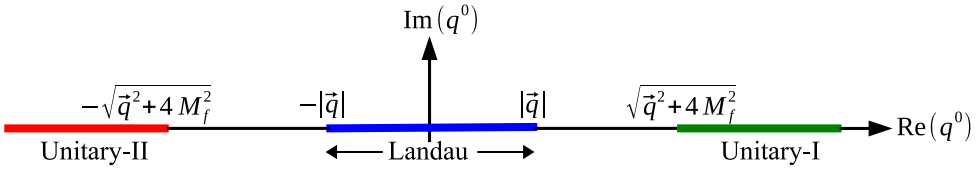

FIG. 2. The branch cuts of $\mathbb{W}_{11}^{\mu\nu}(q)$ in the complex q^0 plane for a given $\vec{q}$. Kinematic domain for the physical dilepton production defined in terms of $q^0 > 0$ and $q^2 > 0$ corresponds to the green region.

$$\mathrm{DPR}_{\mu_5=0} = \left(\frac{dN}{d^4x d^4q}\right)_{\mu_5=0} = \sum_f \Theta(q^2-4m_L^2)\Theta(q^2-4M_f^2) N_c \frac{e^2e_f^2}{192\pi^6}\frac{1}{\beta|\vec{q}|}\left(\frac{1}{e^{\beta q^0}-1}\right)$$
$$\times\left(1+\frac{2m_L^2}{q^2}\right)\sqrt{1-\frac{4m_L^2}{q^2}}\left(1+\frac{2M_f^2}{q^2}\right)\ln\left[\left\{\frac{e^{\beta(q^0+q_-)}+1}{e^{\beta(q^0+q_+)}+1}\right\}\left(\frac{e^{\beta q_+}+1}{e^{\beta q_-}+1}\right)\right], \tag{23}$$

where $q_\pm = -\frac{1}{2}\left[q^0 \pm |\vec{q}|\sqrt{1-\frac{4M_f^2}{q^2}}\right] + \mu_B/3$. The step functions in the above expression restrict the production of dileptons with invariant mass $q^2 < 4m_L^2$ and $q^2 < 4M_f^2$.

B. DPR at $\mu_5 \neq 0$

This subsection is devoted to the evaluation of $g_{\mu\nu}\mathrm{Im}\mathbb{W}_{11}^{\mu\nu}(q)$ in a medium in the presence of chiral imbalance. Here, one needs the 11-component of the real-time thermal quark propagator with finite values of CCP. In the spectral representation this can be expressed as [33,60]

$$S_{11}^f(p) = \int_{-\infty}^{\infty}\frac{dp_0'}{2\pi}\sigma^f(p_0',\vec{p})\left[\frac{1}{p_0'-p_0-i\varepsilon} - 2\pi i\eta(p_0')\delta(p_0'-p_0)\right]$$
$$= \int_{-\infty}^{\infty}\frac{dp_0'}{2\pi}\sigma^f(p_0',\vec{p})\left[\mathcal{P}\left(\frac{1}{p_0'-p_0}\right) - 2\pi i\left(\eta(p_0')-\frac{1}{2}\right)\delta(p_0'-p_0)\right], \tag{24}$$

where the fermionic spectral function $\sigma^f(p_0,\vec{p})$ in the presence of CCP is

$$\sigma^f(p_0,\vec{p}) = 2\pi\mathrm{sgn}(p_0)\frac{\mathcal{D}(p;M_f)}{\omega_p^{+2}-\omega_p^{-2}}[\delta(p^2-\omega_p^{+2})-\delta(p^2-\omega_p^{-2})], \tag{25}$$

in which $\omega_p^r = \sqrt{(|\vec{p}|+r\mu_5)^2+M_f^2}$ with r corresponding to the helicity of the propagating fermion and $\mathcal{D}(p;M_f)$ contains the complicated Dirac structure as

$$\mathcal{D}(p;M_f) = \sum_{j\in\{\pm\}}\mathcal{P}_j[p_{-j}^2\not{p}_j - M_f^2\not{p}_{-j} + M_f(p_j\cdot p_{-j}-M_f^2) + iM_f\sigma_{\mu\nu}p_j^\mu p_{-j}^\nu]. \tag{26}$$

In the above equation, $\mathcal{P}_j = \frac{1}{2}(1+j\gamma^5)$, $p_j^\mu \equiv (p^0+j\mu_5,\vec{p})$ and $\eta(x)$ is already defined in Eq. (21). Using this we get

$$\mathbb{W}_{11}^{\mu\nu} = -i\sum_f e_f^2\int\frac{d^4k}{(2\pi)^4}\int_{-\infty}^{\infty}\frac{dk_0'}{2\pi}\int_{-\infty}^{\infty}\frac{dp_0'}{2\pi}\frac{\mathcal{N}^{\mu\nu}(k,q)\mathrm{sgn}(k_0')\mathrm{sgn}(p_0')}{(\omega_k^{+2}-\omega_k^{-2})(\omega_p^{+2}-\omega_p^{-2})}\{\delta(k^2-\omega_k^{+2})-\delta(k^2-\omega_k^{-2})\}$$
$$\times\{\delta(p^2-\omega_p^{+2})-\delta(p^2-\omega_p^{-2})\}\left[\frac{1-\eta(k_0')}{k_0'-k_0-i\varepsilon}+\frac{\eta(k_0')}{k_0'-k_0+i\varepsilon}\right]\left[\frac{1-\eta(p_0')}{p_0'-p_0-i\varepsilon}+\frac{\eta(p_0')}{p_0'-p_0+i\varepsilon}\right], \tag{27}$$

with $\mathcal{N}^{\mu\nu}(k,q) = \mathrm{Tr}_d[\gamma^\nu\mathcal{D}(p)\gamma^\mu\mathcal{D}(k)]$. Now, contracting $\mathbb{W}_{11}^{\mu\nu}$ with the metric tensor and concentrating on the imaginary part, we get

$$
\begin{aligned}
g_{\mu\nu}\mathrm{Im}\mathbb{W}_{11}^{\mu\nu}(q_0,\vec{q}) = -N_c\sum_f e_f^2\pi\int\frac{d^3k}{(2\pi)^3}\sum_{r\in\{\pm\}}\sum_{s\in\{\pm\}}\frac{1}{16rs\mu_5^2|\vec{p}||\vec{k}|}\frac{1}{4\omega_k^r\omega_p^s}\\
\times[\mathcal{N}(k^0=-\omega_k^r)\{1-f_-(\omega_k^r)-f_+(\omega_p^s)+2f_-(\omega_k^r)f_+(\omega_p^s)\}\delta(q_0-\omega_k^r-\omega_p^s)\\
+\mathcal{N}(k^0=\omega_k^r)\{1-f_+(\omega_k^r)-f_-(\omega_p^s)+2f_+(\omega_k^r)f_-(\omega_p^s)\}\delta(q_0+\omega_k^r+\omega_p^s)\\
+\mathcal{N}(k^0=\omega_k^r)\{-f_+(\omega_k^r)-f_+(\omega_p^s)+2f_+(\omega_k^r)f_+(\omega_p^s)\}\delta(q_0+\omega_k^r-\omega_p^s)\\
+\mathcal{N}(k^0=-\omega_k^r)\{-f_-(\omega_k^r)-f_-(\omega_p^s)+2f_-(\omega_k^r)f_-(\omega_p^s)\}\delta(q_0-\omega_k^r+\omega_p^s)],
\end{aligned}
\tag{28}
$$

where

$$
\begin{aligned}
\mathcal{N}(q,k) = g_{\mu\nu}\mathcal{N}^{\mu\nu} = 16M_f^6 - 4M_f^4\{4(k_+\cdot k_-)+(k_+\cdot p_+)+(k_-\cdot p_-)+4(p_+\cdot p_-)\}\\
+4M_f^2\{(k_+\cdot p_-)(k_-^2+p_+^2)+(k_-\cdot p_+)(k_+^2+p_-^2)+4(k_+\cdot k_-)(p_+\cdot p_-)\}\\
-4\{k_-^2(k_+\cdot p_+)p_-^2+k_+^2(k_-\cdot p_-)p_+^2\}.
\end{aligned}
\tag{29}
$$

Here, some discussions related to the analytic structure of $\mathrm{Im}\mathbb{W}_{11}$ in the complex q_0 plane are in order. It can be seen that, in the presence of finite μ_5, the imaginary part of the matter tensor consists of 16 Dirac delta functions which leads to several branch cuts in the complex q_0 plane. The terms containing $\delta(q_0-\omega_k^r-\omega_p^s)$ and $\delta(q_0+\omega_k^r+\omega_p^s)$ are referred to as Unitary-I and Unitary-II cuts, respectively, as already mentioned in the previous section. However, in the nonzero CCP case each of the Unitary cuts consist of further subcuts owing to the different helicities (r,s). These different cuts correspond to different physical processes. For example, the Unitary-I (Unitary-II) cuts represent the decay of a virtual photon having positive (negative) energy to a real quark-antiquark pair (and the corresponding time-reversed process). The terms with the remaining two delta functions, i.e., $\delta(q_0+\omega_k^r-\omega_p^s)$ and $\delta(q_0-\omega_k^r+\omega_p^s)$, are called Landau-I and Landau-II cuts which also contain four subcuts corresponding to distinct helicities. As already mentioned, Landau cuts stand for the emission (absorption) processes in which a real quark/antiquark in the thermal medium emits (absorbs) a virtual photon. The detailed analysis to find out respective kinematic domains such that the imaginary part of $\mathbb{W}_{11}$ receives nontrivial contributions from the 16 different delta functions has been done in [33]. Here we only quote the final result in tabular form in Eq. (30).

Cuts	Kinematic Regions
Unitary-I	$2M_f \le q_0 < \infty$ for $\lvert\vec{q}\rvert < 2\mu_5$ $\sqrt{(\lvert\vec{q}\rvert-2\mu_5)^2+4M_f^2} \le q_0 < \infty$ for $\lvert\vec{q}\rvert \ge 2\mu_5$
Unitary-II	$-\infty < q_0 \le -2M_f$ for $\lvert\vec{q}\rvert < 2\mu_5$ $-\infty < q_0 \le -\sqrt{(\lvert\vec{q}\rvert-2\mu_5)^2+4M_f^2}$ for $\lvert\vec{q}\rvert \ge 2\mu_5$
Landau-I & Landau-II	$-\lvert\vec{q}\rvert-2\mu_5 \le q_0 \le \lvert\vec{q}\rvert+2\mu_5$

(30)

The pictorial representation of the complex analytical structure of $\mathrm{Im}\mathbb{W}_{11}^{\mu\nu}$ expressed in Eq. (30) is shown in Fig. 3. Since we are interested in physical dileptons, we will restrict ourselves to the timelike kinematic domains with $q_0>0$ and $q^2>0$. From Fig. 3 it is evident, in addition to the Unitary-I cut, that some portion of the Landau cuts $|\vec{q}|<q_0<2\mu_5$ will also contribute to the $g_{\mu\nu}\mathrm{Im}\mathbb{W}_{11}^{\mu\nu}$, and hence to the DPR. This contribution at a lower invariant mass region is purely a finite CCP effect. Moreover, notice that the thresholds of the Unitary cuts strongly depend on μ_5 and M_f. Consequently, for $\mu_5 \ge |\vec{q}|/2$, a positive-energy photon with $q^2 \ge 4(M_f^2-\mu_5^2)$ can, in principle, decay into a real

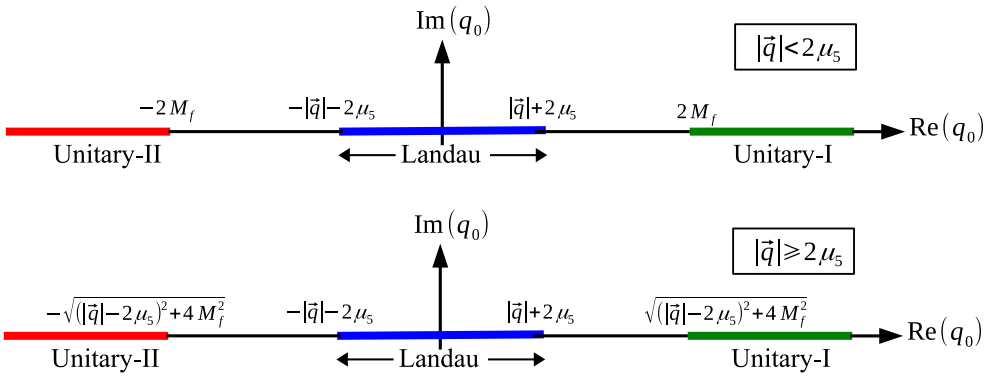

FIG. 3. The branch cuts of the self energy in the complex q_0 plane for a given $|\vec{q}|$ when $|\vec{q}| < 2\mu_5$ (upper panel) and $|\vec{q}| \geq 2\mu_5$ (lower panel). Kinematic domain for the physical dilepton production defined in terms of $q^0 > 0$ and $q^2 > 0$ corresponds to the green region and some portion of the blue region.

quark-antiquark pair below the usual threshold of pair production, $q^2 \geq 4M_f^2$; even for a spacelike photon. Finally, for sufficiently high μ_5, the forbidden gap between the Unitary and Landau cut contributions will vanish irrespective of the value of M_f which enables the production of a continuous spectrum of dileptons throughout the whole range of invariant mass, which is again possible only in a chirally asymmetric medium.

Now, substituting Eqs. (19) and (28) in Eq. (18), we get

$$\begin{aligned}\mathrm{DPR}_{\mu_5\neq 0} = \left(\frac{dN}{d^4x d^4q}\right)_{\mu_5\neq 0} &= \frac{e^2q^2}{4\pi}\left(1+\frac{2m_L^2}{q^2}\right)\sqrt{1-\frac{4m_L^2}{q^2}}\Theta(q^2-4m_L^2)N_c\sum_f e_f^2\pi\int\frac{d^3k}{(2\pi)^3}\sum_{r\in\{\pm\}}\sum_{s\in\{\pm\}}\frac{1}{16rs\mu_5^2|\vec{p}||\vec{k}|}\\
&\times\frac{1}{4\omega_k^r\omega_p^s}[\mathcal{N}(k^0=-\omega_k^r)\{1-f_-(\omega_k^r)-f_+(\omega_p^s)+2f_-(\omega_k^r)f_+(\omega_p^s)\}\delta(q_0-\omega_k^r-\omega_p^s)\\
&+\mathcal{N}(k^0=\omega_k^r)\{1-f_+(\omega_k^r)-f_-(\omega_p^s)+2f_+(\omega_k^r)f_-(\omega_p^s)\}\delta(q_0+\omega_k^r+\omega_p^s)\\
&+\mathcal{N}(k^0=\omega_k^r)\{-f_+(\omega_k^r)-f_+(\omega_p^s)+2f_+(\omega_k^r)f_+(\omega_p^s)\}\delta(q_0+\omega_k^r-\omega_p^s)\\
&+\mathcal{N}(k^0=-\omega_k^r)\{-f_-(\omega_k^r)-f_-(\omega_p^s)+2f_-(\omega_k^r)f_-(\omega_p^s)\}\delta(q_0-\omega_k^r+\omega_p^s)].\end{aligned}\tag{31}$$

In Eq. (31), the angular $d(\cos\theta)$ integral is performed using the Dirac delta functions present in the integrand and the azimuthal $d\phi$ integral gives a factor of 2π. However, unlike the vanishing CCP case, here the analytical evaluation of the remaining $d|\vec{k}|$ integral becomes cumbersome and hence will be evaluated numerically to obtain the DPR. Note that, while calculating the DPR, the constituent quark mass (M_f) for different flavor, which depends on the external parameters such as temperature, BCP, and CCP, are required. Here a NJL model is used to calculate the M_f in different physical conditions.

III. THE CONSTITUENT QUARK MASS USING THE THREE-FLAVOR NAMBU–JONA-LASINIO MODEL

In this section we briefly outline a few important steps to calculate constituent quark mass using the NJL model. The Lagrangian for the three-flavor gauged NJL model is given by

$$\begin{aligned}\mathcal{L} &= \bar{\mathrm{q}}(x)(i\partial\!\!\!/ - eQA\!\!\!/ - \hat{m} + \gamma^0\mu_q + \gamma^0\gamma^5\mu_5)\mathrm{q}(x)\\
&+ G_S\sum_{a=0}^{8}\{(\bar{\mathrm{q}}(x)\lambda^a\mathrm{q}(x))^2 + (\bar{\mathrm{q}}(x)i\gamma_5\lambda^a\mathrm{q}(x))^2\}\\
&- K[\det\bar{\mathrm{q}}(1+\gamma_5)\mathrm{q} + \det\bar{\mathrm{q}}(1-\gamma_5)\mathrm{q}].\end{aligned}\tag{32}$$

In the above expression, $\mathrm{q} = (u\,d\,s)^T$ is the quark field multiplet with three flavors ($N_f = 3$) and three colors ($N_c = 3$) (flavor and color indices are suppressed). $\hat{m} = \mathrm{diag}(m_u, m_d, m_s)$ is the current quark mass matrix. λ^as are the Gell-Mann matrices corresponding to the flavor $SU_f(3)$. The isospin symmetry on the Lagrangian level is assumed, i.e., $m_u = m_d = m_0$, while $SU_f(3)$ symmetry is explicitly broken, so that $m_s \neq m_0$. G_S is the scalar coupling strength and the K term represents the six-point Kobayashi-Maskawa-t'Hooft interaction which is responsible for the breaking of the axial $U(1)_A$ symmetry [63]. Using mean field approximation, one arrives at the following gap equations:

TABLE I. Parameter set for three-flavor model.

$m_u = m_d$ (MeV)	m_s (MeV)	Λ (MeV)	$G_s\Lambda^2$	$K\Lambda^5$
5.1	133	604.5	3.25	10.58

$$M_u = m_u - 2G_s\langle\bar{q}q\rangle_u + 2K\langle\bar{q}q\rangle_d\langle\bar{q}q\rangle_s, \quad (33)$$

$$M_d = m_d - 2G_s\langle\bar{q}q\rangle_d + 2K\langle\bar{q}q\rangle_s\langle\bar{q}q\rangle_u, \quad (34)$$

$$M_s = m_s - 2G_s\langle\bar{q}q\rangle_s + 2K\langle\bar{q}q\rangle_u\langle\bar{q}q\rangle_d, \quad (35)$$

where

$$\langle\bar{q}q\rangle_f = -N_c M_f \sum_r \int \frac{d^3\vec{p}}{(2\pi)^3}\frac{1}{\omega_p^r}\{1 - f_+(\omega_p^r) - f_-(\omega_p^r)\}. \quad (36)$$

The self-consistent solution of Eqs. (33)–(35) results in T and/or μ_B dependence of M_u, M_d, and M_s for different values of CCP. Notice that the medium independent integral, Eq. (36), is ultraviolet divergent. Since the NJL Lagrangian is known to be nonrenormalizable owing to the pointlike interaction between the quarks [63], one has to specify a proper regularization scheme.

To avoid a cutoff artifact, several smooth regularization procedures have been used in the literature by introducing a form factor f_Λ into the diverging vacuum integrals. One can choose a different functional form of this f_Λ, such as the Lorentzian-type form factors [33,67,70,78–80] and the Woods-Saxon-type form factors [81–83]. In this work, we have used first a kind of smoothing function by introducing a multiplicative form factor [33,67,84],

$$f_\Lambda(p) = \sqrt{\frac{\Lambda^{2N_\Lambda}}{\Lambda^{2N_\Lambda} + |\vec{p}|^{2N_\Lambda}}}. \quad (37)$$

In the limit $N_\Lambda \to \infty$, the form factor is reduced to the sharp cutoff function $\Theta(\Lambda - |\vec{p}|)$ which infers that for larger values of N_Λ, the cutoff artifacts are expected to increase. On the other hand, for small N_Λ values, it is impossible to fit different phenomenological values (such as the pion decay constant, the vacuum value of chiral condensate, etc. [79]). Here, we have taken $N_\Lambda = 10$ for numerical convenience. The other model parameters are given in Table I.

These parameters are determined by fitting f_π, m_π, m_K, and $m_{\eta'}$ to their phenomenological values [84].

IV. NUMERICAL RESULTS

In this section, we present the numerical results for constituent quark masses of different flavors which are the main inputs while calculating the DPR from a chirally asymmetric hot and dense medium. In Fig. 4, we have shown the variation of constituent mass of "up" and "strange" quarks as a function of temperature for different values of BCP and CCP which are evaluated by solving Eqs. (33)–(35) self-consistently. One can observe that the spontaneous breaking of the chiral symmetry at small values of temperature results in large values of constituent mass for both "up" and "strange" quarks owing to the large values of quark condensate for all the cases. Now, as the temperature is increased, the constituent mass of the low-lying quarks remains constant up to a certain value of temperature, then falls off sharply in a small range of temperature, and finally becomes nearly equal to the bare masses of the quarks at high T values representing the pseudochiral phase transition due to the (partial) restoration of the chiral symmetry. However, the strange quark mass decreases smoothly when compared to that of the up quark and it can be seen that even at $T \sim 250$ MeV the s-quark mass is still substantially higher than its current mass. The explanation of this behavior comes from Eq. (36). As the current quark mass becomes large, the excitation probability of the quark-antiquark pair becomes thermally suppressed, which leads to a small T-dependence of $\langle\bar{s}s\rangle$ when compared to the low-lying quarks [85]. Now at high temperature as the condensates of u- and d-quarks melt, the third term of Eq. (35) becomes negligible and the constituent mass of the strange quark is solely determined by the $\langle\bar{s}s\rangle$ condensate, resulting in a smooth variation of M_s. This indicates that $SU(3)_f$ symmetry is not even a good approximate symmetry at temperatures larger than 200 MeV, which may be due to the fact that the restoration of the chiral symmetry in the different quark sectors is achieved quite differently [86]. Now, for finite values of BCP, it is seen that the qualitative behaviour of the T-dependence of the u- and s-quark masses remain same, although the transition temperature is found to decrease, thus mimicking the conjectured QCD phase diagram. In the

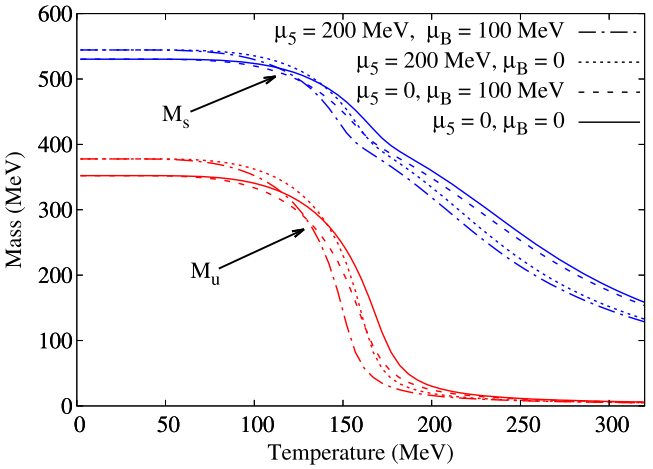

FIG. 4. Constituent quark mass as a function of temperature for different values of μ_B and μ_5. M_u and M_s are represented, respectively, by the red and blue curves.

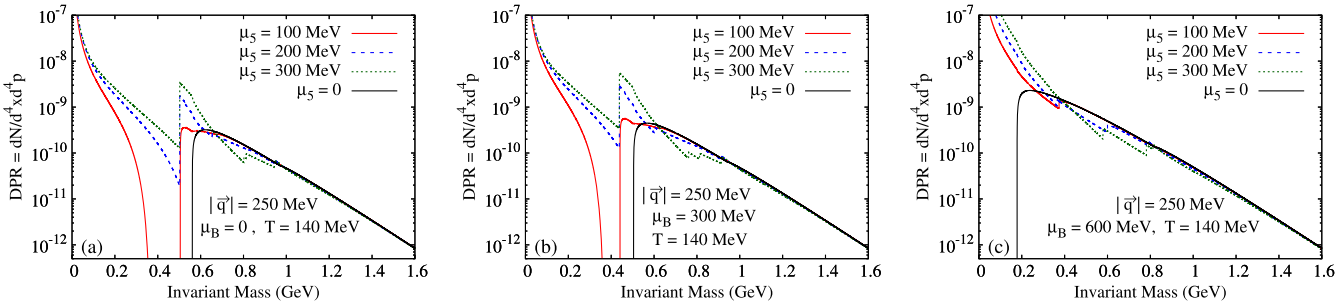

FIG. 5. Dilepton production rate at $|\vec{q}| = 250$ MeV, $T = 140$ at (a) $\mu_B = 0$, (b) $\mu_B = 300$ MeV, and (c) $\mu_B = 600$ MeV, respectively, for different values of μ_5. The DPRs at $\mu_5 = 0$ are also shown for comparison.

presence of finite CCP, the constituent mass of both u- and s-quarks are found to increase in the low temperature region, indicating an enhancement in the magnitude of the quark condensate at small values of T. However, the transition from chirality broken to the restored phase occurs at relatively smaller values of temperature which shows that, at high values of temperature, the formation of the quark condensate is hindered by the presence of finite μ_5, an exact opposite result compared to the low temperature values. These phenomena can be termed as "chiral catalysis" and "inverse chiral catalysis," respectively [33].

Next, we present the numerical results for the DPR from a hot and dense medium in the presence of chiral imbalance. Note that all the results shown hereafter are obtained by ignoring the lepton mass, i.e., $m_L = 0$, and considering the momentum $|\vec{q}| = 250$ MeV. In Fig. 5(a) we have depicted DPRs as a function of invariant mass at $T = 140$ MeV and $\mu_B = 0$ for different values of CCP. The DPR at $\mu_5 = 0$ (black solid line) is also shown for comparison. For the $\mu_5 = 0$ case, the DPR is restricted to low values of invariant mass, as already discussed in Sec. II A. The nontrivial contribution starts from just below 600 MeV owing to the Unitary-I cut threshold $\sqrt{q} \geq 2M_u$. Now from Fig. 4 one can observe that the constituent mass of u-quark at $T = 140$ MeV is ∼290 MeV. This explains the behavior in the case of vanishing CCP. However, in the case of $\mu_5 = 100$ MeV a significant enhancement in the DPR can be seen, owing to nontrivial Landau cut contributions. From Eq. (30), one can observe that the Landau cut contribution will be finite for physical dileptons when $q_0 \leq |\vec{q}| + 2\mu_5$. This can be rewritten as $\sqrt{q^2} \leq 2\sqrt{\mu_5^2 + |\vec{q}|\mu_5}$. For $\mu_5 = 100$ MeV, $2\sqrt{\mu_5^2 + |\vec{q}|\mu_5} \simeq 0.374$ GeV. So, around that value of invariant mass the Landau cut contribution should end, which can be seen in Fig. 5(a) (solid red line). Moreover, the Unitary cut contributions starts at a lower value of invariant mass than the $\mu_5 = 0$ case, although the constituent mass M_u is higher due to the presence of finite CCP. To understand this, let us concentrate on the Unitary cut thresholds for the production of physical dileptons. From Eq. (30), this is expressed as $q^0 \geq \sqrt{(|\vec{q}| - 2\mu_5)^2 + 4M_f^2}$, which can be simplified further to arrive at $\sqrt{q^2} \geq 2\sqrt{\mu_5^2 + M_f^2 - \mu_5|\vec{q}|}$. At $T = 140$ MeV, the constituent mass of the u-quark is ≃283 MeV. So for $\mu_5 = 100$ MeV, the Unitary cut contribution starts at $\sqrt{q^2} \simeq 0.51$ GeV, which is evident from Fig. 5(a). This indicates that a chirally asymmetric medium can induce pair production at comparatively lower values of invariant mass, as discussed in Sec. II B. It also explains the forbidden gap between the Landau and Unitary cut where dilepton production ceases to occur. Now, from the two above discussions about the kinematic domain of the Landau (Unitary) cut, it is clear that as we increase μ_5 the threshold for dilepton production moves towards higher (lower) values of invariant mass. Consequently, for higher values of CCP, i.e., $\mu_5 = 200$ and 300 MeV, the Unitary and Landau cut contributions merge with each other, resulting a continuous spectrum of dileptons for the whole range of invariant mass. In Fig. 5(b) we have presented DPRs as a function of invariant mass at $T = 140$ MeV considering a finite baryon density ($\mu_B = 300$ MeV) for four different values of μ_5. Notice that for the $\mu_5 = 100$ MeV plot (solid red line) the Landau cut threshold ends at the same value as in the zero baryon density case. This is understandable from the fact that the Landau cut threshold only depends on μ_5. However, the Unitary cut threshold, which is directly related to the constituent mass of quarks, moved toward lower values of invariant mass. This can be explained from Fig. 4 where one can observe that for finite values of μ_B the (pseudo)chiral transition temperature moves toward the lower values of T, resulting in a decrease in the magnitude of M_u. In Fig. 5(b), we find a continuous dilepton spectrum for higher values of μ_5 which can be understood in a similar fashion as discussed earlier. In Fig. 5(c), we have considered an even higher baryon density ($\mu_B = 600$ MeV), keeping all the other parameters same as in Figs. 5(a) and 5(b). From the plot of the vanishing CCP case, it is evident that the constituent mass of low lying quarks have decreased further, such that the Unitary cut threshold for $\mu_5 = 0$ is already below the Landau cut threshold for $\mu_5 = 100$ MeV. As a consequence, we get a continuous

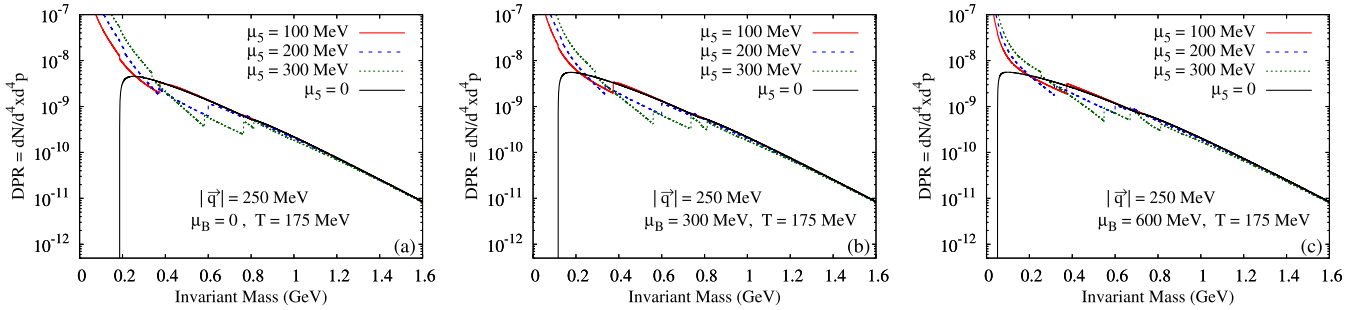

FIG. 6. Dilepton production rate at $|\vec{q}| = 250$ MeV, $T = 175$ at (a) $\mu_B = 0$, (b) $\mu_B = 300$ MeV, and (c) $\mu_B = 600$ MeV, respectively, for different values of μ_5. The DPRs at $\mu_5 = 0$ are also shown for comparison.

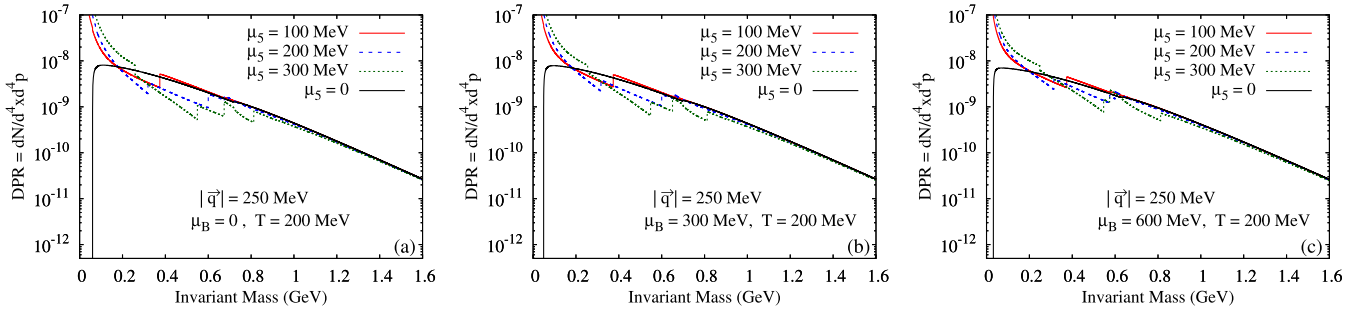

FIG. 7. Dilepton production rate at $|\vec{q}| = 250$ MeV, $T = 200$ at (a) $\mu_B = 0$, (b) $\mu_B = 300$ MeV, and (c) $\mu_B = 600$ MeV, respectively, for different values of μ_5. The DPRs at $\mu_5 = 0$ are also shown for comparison.

spectrum of dileptons for the whole range of invariant mass for all values of CCP shown in the figure.

In Figs. 6(a)–6(c) we have depicted DPRs as a function of invariant mass at $T = 175$ MeV for different values of CCP for $\mu_B = 0$, 300, and 600 MeV, respectively. Considering the zero baryon density case [Fig. 6(a)], it can be seen that, the Unitary cut threshold for $\mu_5 = 0$ is already below the Landau cut threshold for $\mu_5 = 100$ MeV (note that, since the Landau cut contribution only depends on μ_5, it will be same as the previous case). Moreover, from Fig. 4, it is clear that, at $T = 175$ MeV, the constituent masses of low-lying quarks are always below $\lesssim$150 MeV. As a result, at $T = 175$ MeV, for all finite μ_5 cases shown in the figure, the Landau and Unitary cut contribution will merge and a continuous spectrum of dileptons will emerge, as evident from Figs. 6(a)–6(c).

A similar trend is visible in Figs. 7(a)–7(c), where the DPR is plotted for $T = 200$ MeV. Here, because of the restoration of chiral symmetry, the constituent mass of the low-lying quarks goes to the bare mass limit (see Fig. 4). Consequently, the threshold of Unitary cut starts at smaller values of the invariant mass. Moreover, since the temperature considered in this case is higher than all the previous cases, the increase in thermal phase space results in a significant enhancement in the overall magnitude of DPRs when compared to Figs. 5(a)–5(c) [74–76].

We end this section with a discussion on the experimental observation of the effects of chiral imbalance on the dilepton spectra. Keeping in mind that dileptons are emitted at all stages of the collision, the DPRs from quark matter, as well as those from ρ and ω decays and other hadronic reactions, have to be evolved in space-time using $(1+3)$-dimensional hydrodynamics (with $\mu_5 \neq 0$). As discussed earlier, chiral imbalance may be created in HICs locally which leads to a continuous spectrum with a distinct shape in the low invariant mass region of the DPR from quark matter. It should be noted that the creation of a local domain with chiral imbalance changes from event to event and the event average value of any μ_5-dependent observable is zero. Thus, the analysis must be done on an event-by-event basis. Now let us consider an event in which a domain with chirally imbalanced quark matter is created. Due to the hydrodynamic expansion it will cool and undergo a transition to hadronic matter which presumably will also be in the P and CP odd phase. If that be the case, there will be an effect of chiral imbalance on the DPR coming from resonance decay and hadronic reactions, as well. Andrianov *et al.* [87] have predicted that such matter will produce an excess of dileptons in the $\rho - \omega$ resonance region. Together with the enhancement of DPR from quark matter in the low invariant mass region (i.e., nonzero yield in the invariant mass range $M \sim 0.2$–0.4 GeV with $\mu_5 \sim$ 200 MeV or higher) seen in this work, the total dilepton yield could explain the observed low mass enhancement seen in the PHENIX experiment [88] for central collisions which cannot be explained by invoking the temperature and density dependent medium modifications of hadronic spectral functions alone.

V. SUMMARY AND CONCLUSION

In this work we studied the dilepton production rate from hot and dense chirally asymmetric matter likely to be produced in relativistic HICs. The electromagnetic spectral function, which is the principal component in the DPR, is found to be modified due to the presence of a CCP. The constituent quark mass which appears in the in-medium propagator is evaluated in a self-consistent manner using a three-flavor NJL model and is also nontrivially affected by the CCP. Specifically, in the presence of μ_5 the quark condensate is found to be enhanced at small values of T while it is hindered at high values of temperature. We have also analyzed the complete analytic structure of the spectral function of the chirality imbalanced medium in the complex energy plane and have found a nontrivial Landau cut in the physical kinematic region signifying additional scattering processes in the medium; a purely finite CCP effect. As a consequence, the DPR acquires contributions from both the Unitary and Landau cuts for production of dileptons with positive energy and timelike four-momentum. Owing to the emergence of the Landau, cut the DPR is highly enhanced in the low invariant mass region compared to the case with a vanishing CCP. It is also found that the Landau cut threshold is independent of the constituent quark mass, though the Unitary cut threshold has a nontrivial dependence on both M_f and μ_5. For small values of T and μ_5, a forbidden gap exists between Unitary and Landau cuts where production of dileptons is kinematically restricted. However, as we increase the CCP at fixed values of T and μ_B the Landau cut threshold moves toward higher invariant mass. As a result the forbidden gap keeps shrinking and eventually they merge with each other, producing a continuous spectrum of dileptons as a function of invariant mass even for small values of temperature where chiral symmetry is still broken. For higher values of temperature and/or BCP the forbidden gap completely disappears and a significant rise in dilepton production rate is observed, owing to the availability of a larger thermal phase space.

ACKNOWLEDGMENTS

N. C., S. S., and P. R. are funded by the Department of Atomic Energy (DAE), Government of India. S. G. is funded by the Department of Higher Education, Government of West Bengal, India.

[1] M. A. Shifman, Sov. Phys. Usp. **32**, 289 (1989).
[2] A. A. Belavin, A. M. Polyakov, A. S. Schwartz, and Y. S. Tyupkin, Phys. Lett. **59B**, 85 (1975).
[3] G. 't Hooft, Phys. Rev. Lett. **37**, 8 (1976).
[4] G. 't Hooft, Phys. Rev. D **14**, 3432 (1976); **18**, 2199(E) (1978).
[5] N. S. Manton, Phys. Rev. D **28**, 2019 (1983).
[6] F. R. Klinkhamer and N. S. Manton, Phys. Rev. D **30**, 2212 (1984).
[7] V. A. Kuzmin, V. A. Rubakov, and M. E. Shaposhnikov, Phys. Lett. **155B**, 36 (1985).
[8] P. B. Arnold and L. D. McLerran, Phys. Rev. D **36**, 581 (1987).
[9] S. Y. Khlebnikov and M. E. Shaposhnikov, Nucl. Phys. **B308**, 885 (1988).
[10] P. B. Arnold and L. D. McLerran, Phys. Rev. D **37**, 1020 (1988).
[11] S. L. Adler, Phys. Rev. **177**, 2426 (1969).
[12] J. S. Bell and R. Jackiw, Nuovo Cimento A **60**, 47 (1969).
[13] L. D. McLerran, E. Mottola, and M. E. Shaposhnikov, Phys. Rev. D **43**, 2027 (1991).
[14] G. D. Moore and M. Tassler, J. High Energy Phys. 02 (2011) 105.
[15] D. E. Kharzeev, L. D. McLerran, and H. J. Warringa, Nucl. Phys. **A803**, 227 (2008).
[16] V. Skokov, A. Yu. Illarionov, and V. Toneev, Int. J. Mod. Phys. A **24**, 5925 (2009).
[17] K. Fukushima, D. E. Kharzeev, and H. J. Warringa, Phys. Rev. D **78**, 074033 (2008).
[18] D. E. Kharzeev and H. J. Warringa, Phys. Rev. D **80**, 034028 (2009).
[19] G. S. Bali, F. Bruckmann, G. Endrodi, Z. Fodor, S. D. Katz, S. Krieg, A. Schafer, and K. K. Szabo, J. High Energy Phys. 02 (2012) 044.
[20] M. Abdallah *et al.* (STAR Collaboration), Phys. Rev. C **105**, 014901 (2022).
[21] X. An *et al.*, Nucl. Phys. **A1017**, 122343 (2022).
[22] R. Milton, G. Wang, M. Sergeeva, S. Shi, J. Liao, and H. Z. Huang, Phys. Rev. C **104**, 064906 (2021).
[23] M. Ruggieri and G. X. Peng, Phys. Rev. D **93**, 094021 (2016).
[24] M. Ruggieri, G. X. Peng, and M. Chernodub, Phys. Rev. D **94**, 054011 (2016).
[25] M. Ruggieri, M. N. Chernodub, and Z.-Y. Lu, Phys. Rev. D **102**, 014031 (2020).
[26] A. Vilenkin, Phys. Rev. D **20**, 1807 (1979).
[27] A. Vilenkin, Phys. Rev. D **22**, 3080 (1980).
[28] D. T. Son and P. Surowka, Phys. Rev. Lett. **103**, 191601 (2009).
[29] Y. Akamatsu and N. Yamamoto, Phys. Rev. Lett. **111**, 052002 (2013).
[30] S. Carignano and C. Manuel, Phys. Rev. D **99**, 096022 (2019).
[31] S. Carignano and C. Manuel, Phys. Rev. D **103**, 116002 (2021).

[32] S. Carignano and M. Buballa, Phys. Rev. D **101**, 014026 (2020).
[33] S. Ghosh, N. Chaudhuri, S. Sarkar, and P. Roy, arXiv:2201.06473.
[34] E. V. Gorbar and I. A. Shovkovy, arXiv:2110.11380.
[35] J. Charbonneau and A. Zhitnitsky, J. Cosmol. Astropart. Phys. 08 (2010) 010.
[36] M. Kaminski, C. F. Uhlemann, M. Bleicher, and J. Schaffner-Bielich, Phys. Lett. B **760**, 170 (2016).
[37] N. Yamamoto, Phys. Rev. D **93**, 065017 (2016).
[38] I. A. Shovkovy, arXiv:2111.11416.
[39] Q. Li, D. E. Kharzeev, C. Zhang, Y. Huang, I. Pletikosic, A. V. Fedorov, R. D. Zhong, J. A. Schneeloch, G. D. Gu, and T. Valla, Nat. Phys. **12**, 550 (2016).
[40] Q. Li and D. E. Kharzeev, Nucl. Phys. **A956**, 107 (2016).
[41] D. E. Kharzeev, Prog. Part. Nucl. Phys. **75**, 133 (2014).
[42] D. E. Kharzeev, J. Liao, S. A. Voloshin, and G. Wang, Prog. Part. Nucl. Phys. **88**, 1 (2016).
[43] X.-G. Huang, Rep. Prog. Phys. **79**, 076302 (2016).
[44] K. Landsteiner, Acta Phys. Pol. B **47**, 2617 (2016).
[45] E. V. Gorbar, V. A. Miransky, I. A. Shovkovy, and P. O. Sukhachov, Low Temp. Phys. **44**, 487 (2018).
[46] M. Joyce and M. E. Shaposhnikov, Phys. Rev. Lett. **79**, 1193 (1997).
[47] H. Tashiro, T. Vachaspati, and A. Vilenkin, Phys. Rev. D **86**, 105033 (2012).
[48] C.-Y. Wong, *Introduction to High-Energy Heavy-Ion Collisions* (World Scientific, Singapore, 1995), .
[49] L. D. McLerran and T. Toimela, Phys. Rev. D **31**, 545 (1985).
[50] K. Kajantie, J. I. Kapusta, L. D. McLerran, and A. Mekjian, Phys. Rev. D **34**, 2746 (1986).
[51] H. A. Weldon, Phys. Rev. D **42**, 2384 (1990).
[52] J. Alam, B. Sinha, and S. Raha, Phys. Rep. **273**, 243 (1996).
[53] J. Alam, S. Sarkar, P. Roy, T. Hatsuda, and B. Sinha, Ann. Phys. (N.Y.) **286**, 159 (2000).
[54] R. Rapp and J. Wambach, Adv. Nucl. Phys. **25**, 1 (2000).
[55] P. Aurenche, F. Gelis, and H. Zaraket, Phys. Rev. D **62**, 096012 (2000).
[56] P. B. Arnold, G. D. Moore, and L. G. Yaffe, J. High Energy Phys. 12 (2001) 009.
[57] R. Rapp and H. van Hees, in *Quark-Gluon Plasma 4* (World Scientific, Singapore, 2010), pp. 111–206.
[58] R. Chatterjee, L. Bhattacharya, and D. K. Srivastava, Lect. Notes Phys. **785**, 219 (2010).
[59] S. Sarkar and S. Ghosh, J. Phys. Conf. Ser. **374**, 012010 (2012).
[60] S. Mallik and S. Sarkar, *Hadrons at Finite Temperature* (Cambridge University Press, Cambridge, 2016).
[61] Y. Nambu and G. Jona-Lasinio, Phys. Rev. **124**, 246 (1961).
[62] Y. Nambu and G. Jona-Lasinio, Phys. Rev. **122**, 345 (1961).
[63] S. P. Klevansky, Rev. Mod. Phys. **64**, 649 (1992).
[64] M. Buballa, Phys. Rep. **407**, 205 (2005).
[65] U. Vogl and W. Weise, Prog. Part. Nucl. Phys. **27**, 195 (1991).
[66] M. Ruggieri, Phys. Rev. D **84**, 014011 (2011).
[67] K. Fukushima, M. Ruggieri, and R. Gatto, Phys. Rev. D **81**, 114031 (2010).
[68] R. L. S. Farias, D. C. Duarte, G. a. Krein, and R. O. Ramos, Phys. Rev. D **94**, 074011 (2016).
[69] J. Chao, P. Chu, and M. Huang, Phys. Rev. D **88**, 054009 (2013).
[70] L. Yu, H. Liu, and M. Huang, Phys. Rev. D **90**, 074009 (2014).
[71] L. Yu, H. Liu, and M. Huang, Phys. Rev. D **94**, 014026 (2016).
[72] N. Chaudhuri, A. Mukherjee, S. Ghosh, S. Sarkar, and P. Roy, arXiv:2111.12058.
[73] A. Bandyopadhyay and S. Mallik, Phys. Rev. D **95**, 074019 (2017).
[74] S. Ghosh and V. Chandra, Phys. Rev. D **98**, 076006 (2018).
[75] S. Ghosh, N. Chaudhuri, S. Sarkar, and P. Roy, Phys. Rev. D **101**, 096002 (2020).
[76] N. Chaudhuri, S. Ghosh, S. Sarkar, and P. Roy, Phys. Rev. D **103**, 096021 (2021).
[77] C. Greiner, N. Haque, M. G. Mustafa, and M. H. Thoma, Phys. Rev. C **83**, 014908 (2011).
[78] R. Gatto and M. Ruggieri, Phys. Rev. D **82**, 054027 (2010).
[79] R. Gatto and M. Ruggieri, Phys. Rev. D **83**, 034016 (2011).
[80] R. Gatto and M. Ruggieri, Lect. Notes Phys. **871**, 87 (2013).
[81] S. Fayazbakhsh and N. Sadooghi, Phys. Rev. D **83**, 025026 (2011).
[82] S. Fayazbakhsh, S. Sadeghian, and N. Sadooghi, Phys. Rev. D **86**, 085042 (2012).
[83] S. Fayazbakhsh and N. Sadooghi, Phys. Rev. D **90**, 105030 (2014).
[84] L. Yu, J. Van Doorsselaere, and M. Huang, Phys. Rev. D **91**, 074011 (2015).
[85] T. Hatsuda and T. Kunihiro, Phys. Lett. B **198**, 126 (1987).
[86] T. Hatsuda and T. Kunihiro, Phys. Rep. **247**, 221 (1994).
[87] A. A. Andrianov, V. A. Andrianov, D. Espriu, and X. Planells, Phys. Lett. B **710**, 230 (2012).
[88] J. Liao, Pramana **84**, 901 (2015).